AGU PUBLICATIONS

Geophysical Research Letters

RESEARCH LETTER
10.1002/2014GL062307

**Key Points:**
- Combining satellite retrievals and modeling gives valuable information
- Volcanic ash source term is constrained by satellite observations
- Estimates of modeled ash concentrations encountered by a commercial aircraft

**Supporting Information:**
- Data S1
- Readme

**Correspondence to:**
N. I. Kristiansen,
nik@nilu.no

**Citation:**
Kristiansen, N. I., A. J. Prata, A. Stohl, and S. A. Carn (2015), Stratospheric volcanic ash emissions from the 13 February 2014 Kelut eruption, *Geophys. Res. Lett.*, *42*, 588–596, doi:10.1002/2014GL062307.

Received 22 OCT 2014
Accepted 29 DEC 2014
Accepted article online 7 JAN 2015
Published online 22 JAN 2015



# Stratospheric volcanic ash emissions from the 13 February 2014 Kelut eruption

**N. I. Kristiansen[1], A. J. Prata[1,2], A. Stohl[1], and S. A. Carn[3,4]**

[1]Norwegian Institute for Air Research, Kjeller, Norway, [2]Nicarnica Aviation, Kjeller, Norway, [3]Department of Geological and Mining Engineering and Sciences, Michigan Technological University, Houghton, Michigan, USA, [4]Department of Mineral Sciences, National Museum of Natural History, Smithsonian Institution, Washington, District of Columbia, USA

**Abstract** Mount Kelut (Indonesia) erupted explosively around 15:50 UT on 13 February 2014 sending ash and gases into the stratosphere. Satellite ash retrievals and dispersion transport modeling are combined within an inversion framework to estimate the volcanic ash source term and to study ash transport. The estimated source term suggests that most of the ash was injected to altitudes of 16–17 km, in agreement with space-based lidar data. Modeled ash concentrations along the flight track of a commercial aircraft that encountered the ash cloud indicate that it flew under the main ash cloud and encountered maximum ash concentrations of $9 \pm 3$ mg m$^{-3}$, mean concentrations of $2 \pm 1$ mg m$^{-3}$ over a period of 10–11 min of the flight, giving a dosage of $1.2 \pm 0.3$ g s m$^{-3}$. Satellite data could not be used directly to observe the ash cloud encountered by the aircraft, whereas inverse modeling revealed its presence.

## 1. Introduction

In the last few years there has been renewed interest in the effects of volcanic ash on commercial aircraft, primarily due to the major economic damage to the airline industry from the grounding of aircraft in Europe during the April–May 2010 eruptions of Eyjafjallajökull, Iceland. The following year, eruptions from Grímsvötn, also in Iceland and Puyehue-Cordón Caulle, in southern Chile, caused flight delays and cancelations due to the danger posed by transported fine ash (particle sizes < 60 μm diameter) from its effects on jet turbine engines [*Casadevall*, 1994]. Volcanic sulfur dioxide ($SO_2$) gas and particulate emissions can also affect the climate [*Robock*, 2000] and can lead to exceedances of air quality limits [*Thorsteinsson et al.*, 2012]. The inherent unpredictability and sporadic nature of volcanic eruptions, together with their global occurrence make satellite remote sensing the only viable tool to monitor and quantify emissions in all areas of the world. As these emissions can be injected throughout the troposphere and into the stratosphere, they can be rapidly spread by the three-dimensional (3-D) winds. Passive infrared (IR) satellite measurements contain limited vertical height information, but this can be obtained by combining the satellite data with transport simulations.

Forecasting the 3-D transport of fine ash is done using volcanic ash transport and dispersion models [*Bonadonna et al.*, 2011]. These models require accurate initialization (a source term), especially for the time-dependent vertical profiles of the mass of ash and gas erupted [*Mastin et al.*, 2009]. The mass eruption rate (MER) is rarely available, even postanalysis, to provide the required initialization, and either some arbitrary choice is made [*Leadbetter and Hort*, 2011] or an empirical relation is used that relates the MER to the observed maximum height of the ash column height [*Sparks et al.*, 1997] but with a large uncertainty [*Mastin et al.*, 2009]. Recognizing this difficulty, *Stohl et al.* [2011] devised an inversion scheme that utilizes satellite observations with the FLEXPART Lagrangian transport model [*Stohl et al.*, 2005] to determine the MER of fine ash and $SO_2$ and provide more accurate simulations. *Eckhardt et al.* [2008] and *Kristiansen et al.* [2010] have successfully used the inversion technique for $SO_2$ emissions from the eruptions of Jebel-at-Tair, Yemen and Kasatochi, Alaska, and also performed [*Kristiansen et al.*, 2012] sensitivity studies to better understand observational and modeling errors. *Moxnes et al.* [2014] used the technique to study the separation of ash and $SO_2$ emissions during the Grímsvötn 2011 eruption. Similar inversion or data assimilation techniques are also being implemented by other researchers [*Boichu et al.*, 2013; *Flemming and Inness*, 2013; *Pelley et al.*, 2014; *Wilkins et al.*, 2014] with the aim of improving ash and/or $SO_2$ forecasts.

Here we use the inversion method of *Stohl et al.* [2011] to infer the ash concentrations from the eruption of Kelut (also referred to as Kelud) in Java, Indonesia, that erupted violently on 13 February 2014. The eruption was ash-rich; injecting ash well into the stratosphere (as we will show) and into the troposphere thereby intersecting commercial aviation air routes. Geostationary IR satellite data from Japan's second Multifunctional Transport Satellite (MTSAT 2) acquired at hourly intervals are used as observational constraints with the FLEXPART model to obtain the fine ash source term, i.e., time-varying vertical profile of the MER. Using this derived MER, a 3-D ash concentration field is simulated and compared with A-train satellite observations as a means of validation. Two main results are established from this work: the amount and spread of ash in the stratosphere are determined and ash concentrations along the flight path of a commercial jet aircraft en route from Perth, Australia, to Jakarta, Indonesia, are quantified. This latter result is of some significance since the aircraft accidentally encountered smaller ash concentrations in a region below the large, spreading umbrella ash cloud—a region that could not be observed by satellite at the time of the encounter. Previous studies of volcanic ash encountered by aircraft include the study by *Witham et al.* [2012] who analyzed six past eruptions between 1982 and 2006. They highlight the uncertainties in their modeled concentrations due to limited knowledge about source term parameters and aircraft encounter locations and flight paths, as well as errors in the driving meteorological data used for their model simulations (particularly coarser data for eruptions in the 1980s and 1990s). Despite uncertainties of orders of magnitude, they find that between all six cases, plausible maximum ash concentrations encountered by the aircraft range between 4 and 200 mg $m^{-3}$. In our study the source term parameters are better established by inverse modeling, the flight path is accurate, and the meteorological data are of high resolution, which all suggest that the uncertainties involved in our study are considerably lower.

## 2. Mount Kelut Eruption

The Kelut stratovolcano (7.93°S, 112.308°E, 1731 m summit elevation), Java, has been the source of some of Indonesia's most deadly eruptions. More than 30 eruptions, typically short but violent with pyroclastic flows and lahars, have been recorded since 1000 A.D. [*Global Volcanism Program (GVP)*, 2014]. Many of the latest major eruptions with volcanic explosivity index (VEI) of 4 [*Newhall and Self*, 1982], in 1919, 1951, 1966, and 1990, caused widespread fatalities and destruction [*GVP*, 2014].

From mid-January 2014, the number of volcanic earthquakes at Kelut increased. On 13 February at 15:50 UTC Badan Nacional Penanggulangan Bencana (BNPB) reported that a major eruption had occurred followed by another large explosion at 16:30 UTC. Ground-based observers had little insight about the ash plume height, but a number of satellite observations (see next section) suggested that material was ejected up to altitudes between 19 and 20 km, and even exceeding 26 km. Ash fall occurred in areas NE, NW, and W, as far as 240 km W-WNW of the volcano [*GVP*, 2014]. Forty flights from several regional airports were canceled and other flights rerouted. Ash fall and tephra 5–8 cm in diameter caused structures to collapse, including schools, homes, and businesses. Over 76,000 people were evacuated. The eruptive activity finally declined during 14–17 February.

## 3. Satellite Observations

MTSAT 2 data were obtained from the Earthquake Research Institute and Institute of Industrial Science, University of Tokyo (W. Takeuchi, http://webgms.iis.u-tokyo.ac.jp/) and ash retrievals performed using the methodologies outlined in *Prata* [1989], *Prata and Grant* [2001], and *Prata and Prata* [2012]. MTSAT 2 (also called Himawari 7), in geostationary orbit at 145°E longitude, carries a multispectral imager, the MTSAT 2 IMAGER (http://www.wmo-sat.info/oscar/instruments/view/219), that provides 4 km spatial resolution IR data and 1 km resolution visible data, at hourly intervals covering a conical region with a total field of view of about 70°. For the purpose of this study, only data from the IR channels with wavelength bands at 10.3–11.3 μm and 11.5–12.5 μm are used. More details about MTSAT 2 and the IMAGER can be found in *Takeuchi et al.* [2007].

The ash retrievals are performed in two steps: first, pixels are identified as containing ash, containing no ash, or being unsuitable for reliable retrievals based on various thresholding tests. Second, retrievals are performed for the ash-identified pixels and a retrieval is reported as successful or as failed. Failed retrievals occur when the IR optical depth is too large (i.e., for a thick opaque ash cloud) or too small (i.e., very

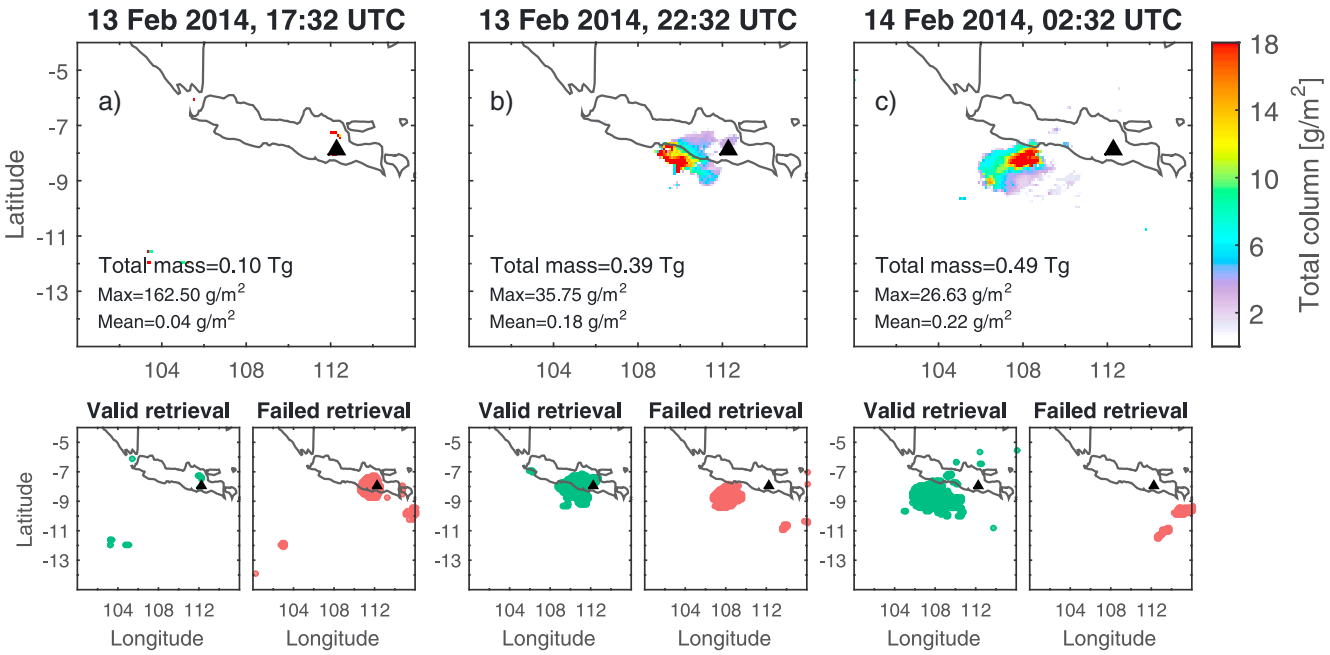


**Figure 1.** Satellite observations: MTSAT ash mass loading retrievals on 13 February 2014 at (a) 17:32, (b) 22:32 and on 14 February 2014 at (c) 02:32 UTC. The large panels show the retrieved ash mass loadings, the smaller panels below show flags for (left) valid retrievals and for (right) failed retrievals. The Kelut volcano is marked by a black triangle.

transparent ash cloud), or possibly due to meteorological clouds likely to contain ice or ice-coated ash which prevent reliable IR ash retrievals. In some cases it is possible to discriminate ice and ash, but in cases where the cloud is opaque the signal is ambiguous. If there was an ash layer below an optically thick ash (or meteorological) cloud, it is effectively masked from the satellite retrievals but, importantly, not necessarily from the inversion scheme, as we demonstrate later. The final product provided to the inversion system consists of a two-dimensional field of flags indicating the type of retrieval (valid ash, no ash, no retrieval, or failed retrieval) along with an ash mass loading for each successful retrieval (Figure 1). The range of mass loadings retrieved by this method varies from 0.2 g $m^{-2}$ to 20 g $m^{-2}$. These lower and upper limits are essentially set by the range of IR optical depths that can be determined.

As well as geostationary data, measurements from several polar-orbiting satellite instruments were available for use in this study. In particular, data from the A-train satellite instruments have been analyzed and used for validation. MODIS (MODerate resolution Imaging Spectroradiomer) data are used to evaluate the plume location and topography, and CALIOP (Cloud-Aerosol Lidar with Orthogonal Polarization) and MLS (Microwave Limb Sounder) data are used to evaluate the vertical location of ash in the stratosphere. We use Level 1 CALIOP Lidar data (CAL_LID_L1-ValStage1-V3-30) obtained from NASA Langley Research Center (https://www-calipso.larc.nasa.gov/search/) and Level 2 MLS data, version 003 (ML2SO2.003, ML2HCL.003, and ML2IWC.003) obtained from the NASA Goddard Earth Sciences Data and Information Services Center (http://disc.sci.gsfc.nasa.gov/Aura/data-holdings/MLS).

## 4. Modeling

The Lagrangian particle dispersion model FLEXPART [*Stohl et al.*, 2005] driven with high-resolution (0.1° × 0.1°) hourly ECMWF (European Centre for Medium-Range Weather Forecasts) analysis data, was used to simulate the transport of volcanic ash in nine particle size bins from 4 to 25 μm diameter and with an assumed density of 2500 kg $m^{-3}$. To determine the ash emissions as a function of altitude and time, the model was used in an inverse modeling framework with a setup almost identical to earlier studies [*Stohl et al.*, 2011; *Kristiansen et al.*, 2012; *Moxnes et al.*, 2014], except for the time and height resolutions of the estimated source term which are here increased along with the resolution of the meteorological data. Unit amounts of ash were released in the model every 30 min from the approximate start time of the eruption reported by BNPB (2014) of 13 February 15:30 UTC until 14 February 22:00 (no later satellite detections of

ash close to the volcano were made), and every 500 m from 2000 m above sea level (asl) up to 35,000 m asl. For the inversion, a total a priori mass emission of 1.5 Tg was distributed uniformly in time and height. However, as an uncertainty of 100 times the a priori emission rate was used, the a priori data were not important for the inversion and the solution was almost entirely driven by the satellite observations. A smoothing condition in time and height was used as an additional constraint.

Twenty-three satellite scenes from 13 February 14:32 UTC until 14 February 12:32 UTC were used with a total number of observations of 23,299 of which 15,874 were zero values and 7425 positive values. Uncertainties in the satellite retrievals were set to 40% [*Wen and Rose*, 1994] with a minimum error bound of 1 g $m^{-2}$. The inversion adjusts the ash emissions as a function of altitude and time such that modeled and observed ash column concentrations are brought into optimal agreement, with a weak additional constraint toward the assumed a priori emission and smoothing condition.

Notice that the satellite observations are mainly sensitive to ash in the size range of about 2.8–28 μm diameter, and thus, our retrieved ash emissions are valid only for this size range [*Stohl et al.*, 2011]. It is likely that total ash emissions were much higher, but the larger particles constituting most of the mass quickly settle out of the atmosphere and are not subject to long-range transport (more than 100–200 km from the vent). However, for the simulations initialized with the estimated source term, the ash particle size distribution (PSD) was extrapolated to larger and smaller ash particle sizes (0.1–250 μm diameter). Sensitivity tests were performed using different extrapolated PSDs. It should be noted that although the satellite ash retrieval is not sensitive to the actual size of the particles and thus their mass for particle diameters greater than about 28 μm, large particles if present in sufficient numbers are always observed because the IR optical depth will be large.

## 5. Results

The MTSAT ash retrievals show that the ash dispersed mainly westward from the volcano (Figure 1) in the hours after the start of the eruption. Maps of the retrieved ash mass loading for the first 8 h include larger regions where the ash retrievals failed (Figures 1a and 1b) due to the thick opaque ash cloud or meteorological clouds. After 14 February 00:32 UTC, when the ash cloud became more dispersed, there are very few failed ash retrievals (Figure 1c).

The source term for fine ash constrained by the MTSAT ash retrievals within the inversion framework is shown in Figures 2b and 2c together with atmospheric sounding measurements at Surabaya airport about 100 km NE of the volcano (Figure 2a). A strong tropopause temperature inversion was located at about 16.5 km (blue line in Figure 2a), and the largest emissions were confined to this altitude level (Figure 2b). Thus, our source term inversion result suggests strong ash detrainment at and slightly above the height of the tropopause, which is a plausible result given the strong static stability of this region. The source term also shows large emissions around 11 and 28 km altitude, without the presence of any temperature inversions at these heights. However, the wind profiles (red and green lines in Figure 2a) show that both wind speed and direction were quite comparable at the three peak emission altitudes. This means that the inversion struggles to distinguish between these emission altitudes and will place ash at all these heights since it was transported in a similar manner. A total of 0.74 Tg of fine ash was released into the atmosphere according to our estimated source term, with about 51% (0.38 Tg) injected into the stratosphere (above the tropopause at 16.5 km).

The temporal variation in the ash emissions (Figure 2c) shows that the strongest emissions occurred in the initial phase of the eruption (15:30–16:00 UTC) and in a later phase from 19:30 to 20:00 UTC, while *GVP* [2014] reported strongest eruptions at 15:50 and 16:30 UTC. Throughout a range of sensitivity tests using alternative setups of the inversion framework (not shown), such as using different amounts of satellite data, start and end time of assumed emission time period, and uncertainties, the major emission altitude around 17 km was a very robust feature. This demonstrates high confidence in this emission altitude while the higher emissions seen around 30 km are more uncertain due to their large variability through the same sensitivity tests.

Several other satellite instruments imaged the ash plume and provided insights into the size, shape, and altitude of the eruption cloud in the atmosphere. About 2 h after the start of the eruption, around 18:10–18:13 UTC, the CALIPSO and Aura satellites overpassed the area and the CALIOP LIDAR and MLS

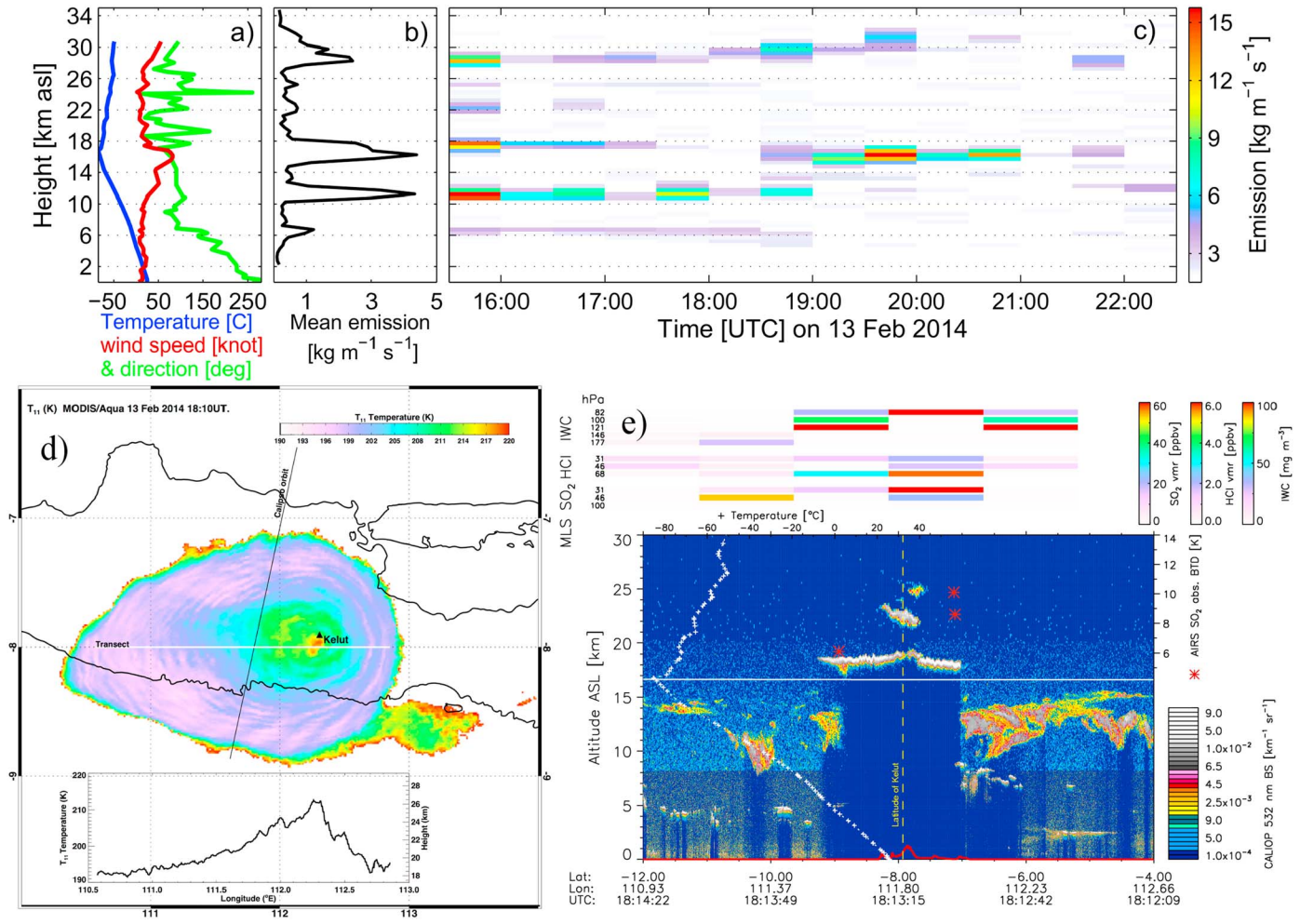


**Figure 2.** Source emissions: (a) Radiosonde sounding data (temperature and wind) from Surabaya Juanda airport at 00:00 UTC on 14 February, (b) vertical source term profile of fine ash optimized from inverse modeling, (c) temporal evolution of the fine ash source term, and (d) MODIS 11 μm thermal image on 13 February 18:10 UTC overlaid with the CALIPSO track (black line). The small inset figure shows the plume topography along the indicated transect (horizontal white line) estimated using single-channel thermal measurements, (e) A-train satellite observations on 14 February at 18:12–18:14 UTC. Curtain plot of CALIOP total attenuated backscatter at 532 nm. Surface topography is shown in red at base of plot and the horizontal white line at 16–17 km indicates the local tropopause. The white crosses are the temperature profile from the Surabaya radiosonde in Figure 2a, and red stars are Atmospheric Infrared Sounder brightness temperature differences indicating the presence of $SO_2$. The latitude of Kelut volcano is also indicated. Above the CALIOP data are collocated MLS $SO_2$, HCl, and ice water content retrievals on several pressure surfaces (hPa).

measured the eruption plume as seen imaged from MODIS very close to the volcano (Figure 2d). The CALIOP measured its strongest signal in altitudes around 17–18 km, with the top of the umbrella cloud at 18–19 km (Figure 2e). This compares well with our major source term altitudes at around 17 km. The small discrepancy of up to 1 km could be attributed to the fact that CALIPSO measured slightly west of the highest altitude portion of the cloud, so it may not have measured the maximum plume altitude, and/or the vertical resolution (about 500 m) of the meteorological data at these altitudes used in the inversion. CALIOP measurements also indicate some higher emissions around 22 and 25 km, and MODIS plume topography estimated using single-channel thermal measurements (Figure 2d, inset) suggests plume tops ranging from about 18 km to 26 km. MLS also detected stratospheric volcanic gases ($SO_2$ and HCl) at pressures of 31–68 hPa (18–22 km altitude), in agreement with the CALIOP data (Figure 2e). This indicates that the emission altitudes between 22 and 26 km by the inversion for the first half hour of the eruption are realistic; however, the source term emissions above 26 km altitude remain uncertain. CALIOP could not detect scatterers below 17 km due to total attenuation of the signal, i.e., no verification of the major emission altitude at 11 km as seen in our estimated source term is possible and it remains uncertain whether it is a realistic feature.

The FLEXPART simulation (Figure 3) initiated with the estimated source term and using an extended PSD shows the main ash cloud being transported westward (Figure 3a) in agreement with the MTSAT ash retrievals for the same time (Figure 1b). The vertical distribution of the modeled ash concentrations as a function of longitude and height (Figure 3b) illustrates that the highest concentrations of ash are in an altitude range of about 12–18 km. It is evident that the ash around 30 km is transported into similar directions as the ash at 10–18 km, illustrating the difficulty of separating these emission heights in the inversion. Notice that the vertical distribution does not show the ash transport along any particular latitude, but is the maximum modeled ash concentrations over all latitudes, and may therefore not give a correct picture of the actual ash transport.

One potential source of uncertainty in the model simulations is the fact that neither the ECMWF nor the FLEXPART model simulate the dynamics of the eruption and the wind field inside the umbrella cloud. However, when the main interest is in long-range transport, the umbrella cloud can be considered subgrid scale (as long as it is not too large), as it mainly affects transport processes in the vicinity of the volcano. The likely effect of neglecting the umbrella in the modeling is a smoothing (in height and time) of the retrieved emission distribution, and hence errors in the exact height and timing of the emissions, but it should not lead to systematic errors.

A commercial jet aircraft en route from Perth, Australia, to Jakarta, Indonesia, accidentally encountered the ash cloud from Mount Kelut. Fumes in the cabin and observation of St. Elmo's Fire alerted the crew to execute avoidance actions (a route change and descent to lower altitude). Figure 3a shows the modeled ash mass loadings at the time of the aircraft encounter overlaid with the flight track in blue, suggesting that the aircraft flew in the western part of the ash cloud. This is also evident from the MTSAT ash retrievals in Figure 1b, although failed ash retrievals occur in the specific area (discussed further in a sensitivity study below). The modeled 3-D ash concentrations were sampled along the flight track to investigate the ash concentration levels that the aircraft potentially encountered. A vertical cross section of the ash concentrations along the flight track (Figure 3c) shows that most of the ash along this track was located above flight altitude. The modeled concentrations along the flight track (Figure 3d) indicate that the aircraft experienced maximum ash concentrations of about $9 \pm 3$ mg m$^{-3}$, with mean ash concentration of $2 \pm 1$ mg m$^{-3}$ over a period of 10–11 min. The corresponding dosage, calculated as the integral of the concentration over time, is $1.2 \pm 0.3$ g s m$^{-3}$. The uncertainties in the concentrations (turquoise bars) are estimated from a range of simulations using different source terms from sensitivity studies (one described below) and different initial PSDs. The modeled PSD (Figure 3e) at the time of the encounter (green line) shows that the particle sizes constituting most of the ash mass are below 20 μm diameter, and the larger particles (20–250 μm diameter) initiated at the volcano source (red line) have settled out. Processes such as ash fall from the umbrella cloud into the altitude of the encounter are important. In one of our sensitivity studies used in the calculation of the uncertainty estimate of Figure 3d, the assumed PSD was shifted to larger particle sizes with a peak at 12 μm diameter and a second smaller peak at 100 μm diameter. The model simulations using this PSD account for more ash fall down to lower altitudes as gravitational settling is enhanced.

The westernmost parts (108–109°E) of the ash cloud, where the aircraft encounter occurred, are somewhat uncertain because the MTSAT ash retrievals suggest a thick opaque ash cloud (or possibly meteorological cloud, likely to be ice or ice-coated ash) in that area (Figure 1b), for which no quantitative ash retrieval could be made. Due to the fact that the failed satellite retrieval values were disregarded in the source term estimate, the modeled ash columns in the same area are relatively low (Figure 3a). The inversion locates some ash there only because this ash was observed elsewhere at a later time. It is highly likely that there was some ash in the area of the failed retrievals in Figure 1. In one sensitivity test we examined how strongly these failed retrieval values affect the source term estimate and the modeled transport. In the test, we spread the ash into the areas with failed retrievals, by manually giving all failed retrievals a high ash mass loading, i.e., 20 g m$^{-2}$. These data were then used in an inversion, and the resulting source term estimate shows strongest ash emissions (not shown) at 16–17 km altitude, similar to our previous source term illustrating the robustness of this emission altitude. But the strongest emissions now occur in a different phase of the eruption (around 17:30 UTC) and are of a greater magnitude. Initializing FLEXPART using this alternative source term produces a much denser ash cloud in the westernmost part (107–109°E) of the cloud. The westernmost ash cloud is located around 16 km altitude, and the modeled ash concentrations

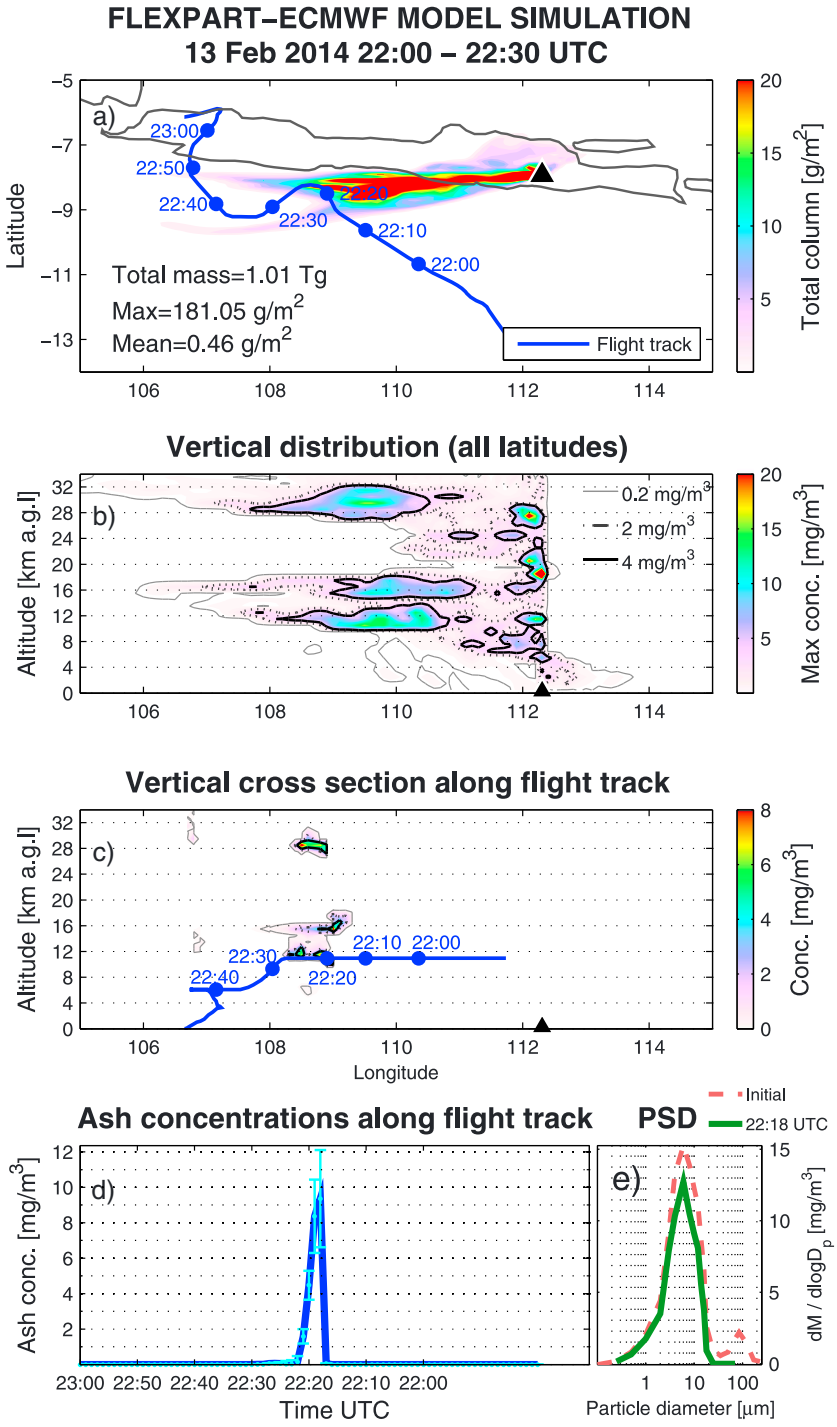


**Figure 3.** Modeled ash clouds: (a) FLEXPART-modeled total ash columns of fine ash. The model is initiated with the estimated source term from Figure 2c and an extended ash particle size distribution (PSD). The blue line is the flight track of the aircraft that encountered the ash cloud, and the Kelut volcano is marked by a black triangle. (b) Modeled vertical distribution of fine ash (the maximum concentrations across all latitudes are shown), (c) modeled vertical cross section along the flight track, (d) modeled ash concentrations, with error bars (turquoise), along the flight track, and (e) the modeled ash PSD at the time of the maximum modeled ash concentration along the flight track at 22:18 UTC and released at the source (initial).

along the flight track showed a maximum of 4 mg $m^{-3}$ which is lower than that for the simulation shown in Figure 3.

We can therefore conclude that the aircraft accidentally encountered volcanic ash in a region below the large, spreading umbrella ash cloud—in a region where quantitative volcanic ash retrievals from satellite data were not possible. The ash contained in this part of the plume could only be measured quantitatively some hours later as it emerged from the umbrella-shaped cloud. While uncertainties in the modeled ash concentrations are high, our best estimate is that the highest ash concentrations encountered by the aircraft were about $9 \pm 3$ mg $m^{-3}$, which is almost twice the limit value for the No-Fly zone of 4 mg $m^{-3}$, set by *European Commission* [2010] during the 2010 Eyjafjallajökull eruption. Even higher ash concentrations were likely present at altitudes above the flight level.

## 6. Conclusions

The Mount Kelut eruption on 13 February 2014 sent ash and gases high into the atmosphere. By combining satellite ash retrievals from MTSAT observations and FLEXPART transport modeling, we estimated the volcanic ash source term and studied the ash transport. Our main results can be summarized as follows:

1. The estimated source term distribution shows that most of the ash was injected to altitudes of around 17 km, in agreement with space-based CALIOP and MODIS data.
2. For the first time, we calculate and report ash mass dosages received by a commercial airliner encountering a volcanic ash cloud. Modeled volcanic ash concentrations along the flight track of the aircraft were found to be $9 \pm 3$ mg $m^{-3}$, with a mean value of $2 \pm 1$ mg $m^{-3}$ over a period of 10–11 min of the flight. This corresponds to a dosage of $1.2 \pm 0.3$ g s $m^{-3}$. The concentration values are close to or exceed the limit value for the No-Fly zone of 4 mg $m^{-3}$, set by the European Commission (2010) during the 2010 Eyjafjallajökull eruption. Phenomena observed by the crew (e.g., fumes in the cabin and St. Elmo's fire) justifiably caused them to perform an avoidance maneuver (route change and descent to a lower altitude).
3. Satellite ash retrievals can be problematic for thick opaque ash clouds or when meteorological clouds with ice coating are present. In this case, quantitative ash retrievals were only possible as the ash emerged from the umbrella-shaped eruption cloud several hours after the eruption. Retrieval failures may be challenging in the source term estimates, making it problematic to reproduce ash clouds, where it is likely that a thick opaque ash cloud is present. While quantitative satellite retrievals cannot be made in these opaque parts of the clouds, it is possible to estimate mass loadings using the optical depth and a priori size distribution assumptions. Also, another possible way to reconstruct ash loadings in areas of failed ash retrievals might be to use UV $SO_2$ data (e.g., Ozone Monitoring Instrument) to calculate $SO_2$/ash ratios where both species were observed, and extend the ash cloud into areas where only $SO_2$ was detected using this ratio. However, for the case of Kelut, the first UV $SO_2$ retrieval was not until Feb 14 at 6:30 UTC, by which time substantial ash fall would have occurred. These issues should be analyzed further and are important to consider in aviation hazard assessments.
4. The method of combining satellite retrievals and transport modeling gives information that cannot be obtained using either data source alone. By constraining the model with satellite data, ash concentrations and calculation of dosages experienced by actual and hypothetical aircraft routes can be estimated with higher accuracy, providing invaluable information to aviation hazard assessments.

**Acknowledgments**

We thank the Japan Meteorological Agency (JMA) and Wataru Takeuchi (University of Tokyo) for supplying the MTSAT 2 data and Manfred Birnfeld (AIRBUS) for helpful advice regarding the aircraft flight track. NASA provided the data from MODIS, CALIOP, and MLS used in this study. This work was partially funded by the European Space Agency under the VAST project. S.A.C. acknowledges support from NASA through the Aura Science Team (grant NNX11AF42G) and MEaSUREs (grant NNX13AF50G) programs. The data used to produce Figure 2c (source term) are provided as supporting information to this manuscript.

The Editor thanks Roger Denlinger and an anonymous reviewer for their assistance in evaluating this paper.

## References

Boichu, M., L. Menut, D. Khvorostyanov, L. Clarisse, C. Clerbaux, S. Turquety, and P.-F. Coheur (2013), Inverting for volcanic $SO_2$ flux at high temporal resolution using spaceborne plume imagery and chemistry-transport modelling: The 2010 Eyjafjallajökull eruption case study, *Atmos. Chem. Phys.*, *13*(17), 8569–8584, doi:10.5194/acp-13-8569-2013.

Bonadonna, C., A. Folch, S. Loughlin, and H. Puempel (2011), Future developments in modelling and monitoring of volcanic ash clouds: Outcomes from the first IAVCEI-WMO workshop on Ash Dispersal Forecast and Civil Aviation, *Bull. Volcanol.*, *74*(1), 1–10, doi:10.1007/s00445-011-0508-6.

Casadevall, T. (1994), The 1989–1990 eruption of Redoubt Volcano, Alaska: Impacts on aircraft operations, *J. Volcanol. Geotherm. Res.*, *62*(1–4), 301–316, doi:10.1016/0377-0273(94)90038-8.

Eckhardt, S., A. Prata, P. Seibert, K. Stebel, and A. Stohl (2008), Estimation of the vertical profile of sulfur dioxide injection into the atmosphere by a volcanic eruption using satellite column measurements and inverse transport modeling, *Atmos. Chem. Phys.*, *8*(14), 3881–3897.

European Commission (2010), *Report on the Actions Undertaken in the Context of the Impact of the Volcanic Ash Cloud Crisis on the Air Transport Industry.* [Available at http://ec.europa.eu/transport/doc/ash-cloud-crisis/2010_06_30_volcano-crisis-report.pdf.]

Flemming, J., and A. Inness (2013), Volcanic sulfur dioxide plume forecasts based on UV satellite retrievals for the 2011 Grímsvötn and the 2010 Eyjafjallajökull eruption, *J. Geophys. Res. Atmos.*, *118*, 10,172–10,189, doi:10.1002/jgrd.50753.

Global Volcanism Program (GVP) (2014), *Smithsonian Institution, Kelut Eruption Page.* accessed Aug 2014. [Available at http://www.volcano.si.edu/volcano.cfm?vn=263280.]

Kristiansen, N. I., et al. (2010), Remote sensing and inverse transport modeling of the Kasatochi eruption sulfur dioxide cloud, *J. Geophys. Res.*, *115*, D00L16, doi:10.1029/2009JD013286.

Kristiansen, N. I., et al. (2012), Performance assessment of a volcanic ash transport model mini-ensemble used for inverse modeling of the 2010 Eyjafjallajökull eruption, *J. Geophys. Res.*, *117*, D00U11, doi:10.1029/2011JD016844.

Leadbetter, S. J., and M. C. Hort (2011), Volcanic ash hazard climatology for an eruption of Hekla Volcano, Iceland, *J. Volcanol. Geotherm. Res.*, *199*(3–4), 230–241, doi:10.1016/j.jvolgeores.2010.11.016.

Mastin, L., et al. (2009), A multidisciplinary effort to assign realistic source parameters to models of volcanic ash-cloud transport and dispersion during eruptions, *J. Volcanol. Geotherm. Res.*, *186*(1), 10–21, doi:10.1016/j.jvolgeores.2009.01.008.

Moxnes, E., N. Kristiansen, A. Stohl, L. Clarisse, A. Durant, K. Weber, and A. Vogel (2014), Separation of ash and sulfur dioxide during the 2011 Grímsvötn eruption, *J. Geophys. Res. Atmos.*, *119*, 7477–7501, doi:10.1002/2013JD021129.

Newhall, C. G., and S. Self (1982), The Volcanic Explosivity Index (VEI): An estimate of explosive magnitude for historical volcanism, *J. Geophys. Res.*, *87*(C2), 1231–1238.

Pelley, R., M. Cooke, A. Manning, D. Thomson, C. Witham, and M. Hort (2014), Inversion technique for estimating emissions of volcanic ash from satellite imagery, Geophysical Research Abstracts EGU2014-12950 paper presented at EGU General Assembly 2014, Vienna, 27 April–2 May.

Prata, A. (1989), Infrared radiative transfer calculations for volcanic ash clouds, *Geophys. Res. Lett.*, *16*(11), 1293–1296, doi:10.1029/GL016i011p01293.

Prata, A., and I. Grant (2001), Retrieval of microphysical and morphological properties of volcanic ash plumes from satellite data: Application to Mt Ruapehu, New Zealand, *Q. J. R. Meteorolog. Soc.*, *127*(576), 2153–2179, doi:10.1002/qj.49712757615.

Prata, A., and A. Prata (2012), Eyjafjallajökull volcanic ash concentrations determined using spin enhanced visible and infrared imager measurements, *J. Geophys. Res.*, *117*, D00U23, doi:10.1029/2011JD016800.

Robock, A. (2000), Volcanic eruptions and climate, in *Volcanism and the Earth's Atmosphere, Geophys. Monogr.*, vol. 139, edited by A. Robock and C. Oppenheimer, pp. 191–219, AGU, Washington, D. C. ISBN: 0-87590-998-1.

Sparks, R. S. J., M. I. Bursik, S. N. Carey, J. S. Gilbert, L. S. Glaze, H. Sigurdsson, and A. W. Woods (1997), *Volcanic Plumes*, 1st ed., 574 pp., John Wiley, Chichester, U. K.

Stohl, A., C. Forster, A. Frank, P. Seibert, and G. Wotawa (2005), Technical note: The Lagrangian particle dispersion model FLEXPART 6.2, *Atmos. Chem. Phys.*, *5*, 2461–2474.

Stohl, A., et al. (2011), Determination of time- and height-resolved volcanic ash emissions and their use for quantitative ash dispersion modeling: The 2010 Eyjafjallajökull eruption, *Atmos. Chem. Phys.*, *11*(9), 4333–4351, doi:10.5194/acp-11-4333-2011.

Takeuchi, W., T. Nemoto, T. Kaneko, and Y. Yasoka (2007), Development of MTSAT data processing, visualization and distribution system on WWW, *J. Jpn. Soc. Photogramm. Remote Sens.*, *46*(6), 42–48.

Thorsteinsson, T., T. Jóhannsson, A. Stohl, and N. Kristiansen (2012), High levels of particulate matter in Iceland due to direct ash emissions by the Eyjafjallajökull eruption and resuspension of deposited ash, *J. Geophys. Res.*, *117*, B00C05, doi:10.1029/2011JB008756.

Wen, S., and W. I. Rose (1994), Retrieval of sizes and total masses of particles in volcanic clouds using AVHRR bands 4 and 5, *J. Geophys. Res.*, *99*(D3), 5421–5431, doi:10.1029/93JD03340.

Wilkins, K., M. Watson, H. Webster, D. Thomson, H. Dacre, S. Mackie, and N. Harvey (2014), Volcanic ash cloud forecasting: Combining satellite observations and dispersion modelling, Geophysical Research Abstracts EGU2014-1615 paper presented at EGU General Assembly, Vienna, 27 April – 2 May.

Witham, C., H. Webster, M. Hort, A. Jones, and D. Thomson (2012), Modelling concentrations of volcanic ash encountered by aircraft in past eruptions, *Atmos. Env.*, *48*, 219–229, doi:10.1016/j.atmosenv.2011.06.073.